Journal of
*Marine Science and Engineering*

MDPI

*Article*

# Atmosphere-Ocean Processes Governing Inflow to the Northern Caribbean Sea

**Mark R. Jury** [1,2]

[1] Physics Department, University of Puerto Rico Mayagüez, Mayaguez, PR 00682, USA; mark.jury@upr.edu
[2] Geography Department, University of Zululand, KwaDlangezwa 3886, South Africa

**Abstract:** Near-surface currents entering the northern Caribbean from the Atlantic are described using ocean reanalysis at monthly to daily timescales, underpinned by satellite data assimilation. Statistical analyses involved spatial clustering into current vector modes with associated time scores for quantifying spectral power and regression onto atmospheric fields. Inflow across the Anegada, Mona, Windward (AMW) Passages peaks at ~100 m depth at ~0.2 m/s during summer and pulses at periods of 45, 100, and 365 days, and at 3, 6.5 years. The intra-seasonal periods may relate to Madden–Julian Oscillations and westward ocean Rossby waves, while inter-annual periods associate with regional climate anomalies. An empirical orthogonal function analysis demonstrates that AMW inflow varies across multiple timescales and is enhanced when the subtropical high-pressure ridge penetrates into the western Caribbean. A case study reveals key features during a surge of inflow to the northern Caribbean. Marine climate change involves heat advected poleward by currents along the western edge of the tropical Atlantic, fed through the Caribbean Sea. Consequently, the study of inflows garners wide interest.

**Keywords:** Caribbean inflow; Atlantic passages; marine climate



**Citation:** Jury, M.R. Atmosphere-Ocean Processes Governing Inflow to the Northern Caribbean Sea. *J. Mar. Sci. Eng.* **2023**, *11*, 718. https://doi.org/10.3390/jmse11040718

Academic Editor: Nikolaos Skliris

Received: 3 March 2023
Revised: 15 March 2023
Accepted: 22 March 2023
Published: 26 March 2023



## 1. Introduction

The northwest Atlantic pathway of the ocean conveyor that sequesters thermal energy [1–4] infiltrates the Caribbean Sea through narrow passages. The basin-scale anticyclonic gyre circulation driven by mid-latitude westerlies and sub-tropical easterlies [5,6] is modulated by the El Nino Southern Oscillation (ENSO) [7–9]. Inflow to the southern Caribbean near Grenada is fed by the North Brazil Current (NBC) [10,11], and exhibits intra-seasonal variability of ~10 Sv due to NBC eddies [12–17]. The Caribbean Current (along 15° N) skirts an upwelling zone off Venezuela and feeds the Yucatan outflow of ~28 Sv that peaks in late summer [18,19]. Some Antilles passages have long-term inflow observations, but most estimates derive from infrequent field surveys constrained by model simulations [20–22].

Caribbean inflow is altered by the wind-driven gyre and meridional overturning circulation involving ~15 Sv inter-hemispheric transfers [23–32]. There are nine main passages in the Antilles arc (cf. Appendix A), including north-facing Antigua, Anegada, Mona, Windward (AMW), which are the focus of this study. Transport in the southeast passages near Grenada is ~10 Sv; the Antigua, Anegada, Mona Passages each draw ~2 Sv from the North Atlantic gyre, while Windward Passage inflow is ~5 Sv [33–38], consistent with a total transport of ~28 Sv. The Caribbean Current feeds these inflows toward the Yucatan Channel that finally loops into the Florida Current.

Here, a statistical exploration of northern Caribbean inflow is presented using upper ocean reanalysis products (cf. Table 1) at monthly and daily intervals. Scientific questions include: (i) what are the characteristics of inflow to the northern Caribbean, (ii) how is inflow variability related to basin currents and winds on inter-annual to intra-seasonal timescales? (iii) what are the local attributes of high and low inflows? And (iv) what are the secondary consequences?

**Table 1.** Listing of datasets.

| Acronym | Name, Version | Horizontal Resolution | Temporal Details | Web-Source |
|---|---|---|---|---|
| ERA5 | European Centre (Atmos.) Reanalysis v5 | 25 km | 1979–2019 daily | Climate Explorer KNMI Univ Hawaii APDRC |
| EU-marine | European Union satellite Altimetry reanalysis | 25 km | 1992–2019 daily | Climate Explorer KNMI |
| GHR SST | Global High-Res. SST via UKMO v1 (IR + MW) | 1 km | 2008–2019 daily | Univ Hawaii APDRC |
| HYCOM3 | Hybrid Coord. Ocean Model v3 reanalysis w/NCODA | 10 km | 2000–2019 daily | Univ Hawaii APDRC |
| NOAA | Nat. Ocean & Atmos. Admin. SST, netOLR | 25 km | 1980–2019 daily | IRI Climate Library |
| SODA3 | Simple Ocean Data Assim. V3 reanalysis w/MERRA2 | 50 km | 1980–2015 monthly | IRI Climate Library |

## 2. Data and Methods

Inflow to the northeastern Caribbean 15–22° N, 78–61° W (Figure 1a) is characterized by upper ocean currents for the period 1980–2015 using monthly Simple Ocean Data Assimilation v3 (SODA3) underpinned by NASA Meteorology v2 hindcasts (MERRA2) [39,40], NOAA sea surface temperature (SST) [41], and satellite microwave observations. The marine climate in the wider region of 6–32° N, 90–50° W is described by NASA net outgoing longwave radiation (net OLR) [42], European Community v5 reanalysis (ERA5) [43] sea level air pressure (SLP), winds, and net heat flux, and EU-marine sea surface height dynamic topography (SSHdt) [44] based on satellite altimetry. Means were calculated for the period 2000–2019 in recognition of improved satellite coverage. Dataset attributes are listed in Table 1. Both monthly SODA3 and daily HYCOM reanalyses have eddy-resolving capability, with uncertainty arising from sampling intervals for infrequent altimetry and cloudy thermal radiance.

To quantify low-frequency fluctuations of inflow to the northern Caribbean, monthly SODA3 zonal (U) and meridional (V) 5–200 m depth-averaged currents were subjected to empirical orthogonal function (EOF) analysis, using an IRI Climate Library subroutine. The co-varying mode-1 U and V currents form a vector pattern and standardized EOF time-score representing temporal variability in the AMW area. The EOF time-score was analyzed for wavelet spectral energy and used in spatial regressions onto regional field anomalies of detrended NOAA SST, NASA netOLR (a proxy for cloud depth), ERA5 SLP, net heat flux, and EU SSHdt. The statistical methods explore variations of inflow by ranking the monthly EOF time-score. The top and bottom ranked cases (cf. Table 2a) were field-averaged, then subtracted to form a 'high minus low inflow' composite, to study regional-scale differences in wind stress, upper-layer currents, and salinity fields.

To characterize high-frequency fluctuations of inflow to the Anegada passage for the period 2000–2019, daily 0.1° HYCOM3 reanalysis [45] of 100 m U and V currents in the area 17.9–18.7° N, 64.0–65.1° W were averaged to form an index (south-westward inflow: positive). The daily Anegada inflow time series was analyzed for wavelet spectral energy, and the peak case of 11–12 February 2001 was studied (Table 2b). As in the monthly analysis, the daily U V inflow time series was employed in spatial regressions onto regional fields of detrended ERA5 SLP, zonal winds, and dewpoint temperature. Point-to-field (or time-to-space) associations were quantified by regression of the inflow time series onto field data.

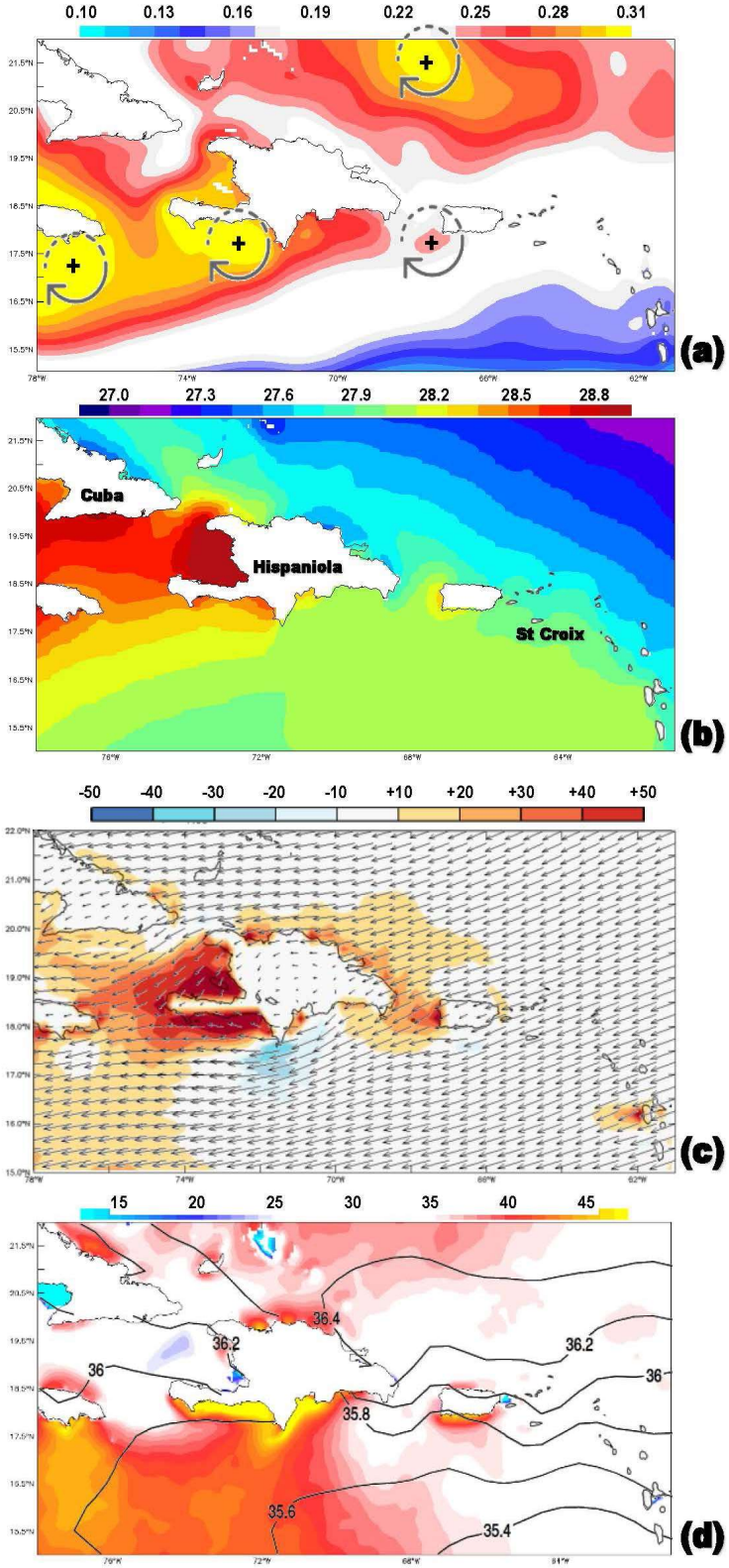


**Figure 1.** Mean annual maps of: (**a**) SSH (m), (**b**) satellite SST (°C), (**c**) ERA5 wind vector and net heat flux (shaded, W/m$^2$) highlighting wind shadows, and (**d**) HYCOM mixed layer depth (shaded, m) and 1–30 m salinity (contours, ppt). Standing anticyclonic eddies labelled + in (**a**); all averaged 2000–2019.

**Table 2.** (**a**) Ranking of monthly AMW inflow based on Figure 2c standardized time-scores. (**b**) Ranking of daily Anegada inflow based on Figure 4b, case study bold.

| (a) | Lowest | | Highest | (b) | Inflow |
|---|---|---|---|---|---|
| Dec-1992 | −1.98 | Jan-1989 | 1.53 | **11-Feb-2001** | 0.67 |
| Jan-1993 | −1.69 | Mar-1989 | 1.55 | 19-Apr-2014 | 0.61 |
| Nov-1992 | −1.60 | Sep-2014 | 1.56 | 10-Feb-2001 | 0.61 |
| Nov-2005 | −1.32 | Sep-2000 | 1.57 | 31-Dec-2010 | 0.60 |
| May-1992 | −1.20 | Feb-1989 | 1.59 | 30-Dec-2010 | 0.60 |
| Dec-2006 | −1.04 | Jun-1988 | 1.60 | **12-Feb-2001** | 0.60 |
| Apr-1992 | −1.01 | May-2000 | 1.66 | 23-Jul-2003 | 0.59 |
| Oct-2005 | −0.98 | Dec-2004 | 1.68 | 21-Apr-2013 | 0.56 |
| Jun-1992 | −0.82 | Feb-1988 | 1.69 | 09-Feb-2001 | 0.56 |
| Feb-1993 | −0.81 | Aug-2003 | 1.77 | 20-Apr-2013 | 0.55 |
| Sep-2005 | −0.74 | Sep-2003 | 1.80 | 22-Jul-2003 | 0.55 |
| Oct-1992 | −0.74 | Feb-2000 | 1.81 | 24-Jul-2003 | 0.54 |
| Mar-1992 | −0.70 | Apr-2000 | 1.95 | 22-Mar-2011 | 0.54 |
| Dec-1989 | −0.70 | May-1988 | 1.95 | 23-Mar-2011 | 0.54 |
| Jun-2005 | −0.69 | Mar-2000 | 1.97 | 12-Jan-2015 | 0.54 |
| May-2005 | −0.68 | Mar-1988 | 2.19 | 18-Apr-2014 | 0.53 |
| Jan-2006 | −0.68 | Apr-1988 | 2.24 | 20-Apr-2014 | 0.53 |
| | | | | 13-Jan-2015 | 0.53 |
| | | | | 17-Mar-2001 | 0.52 |

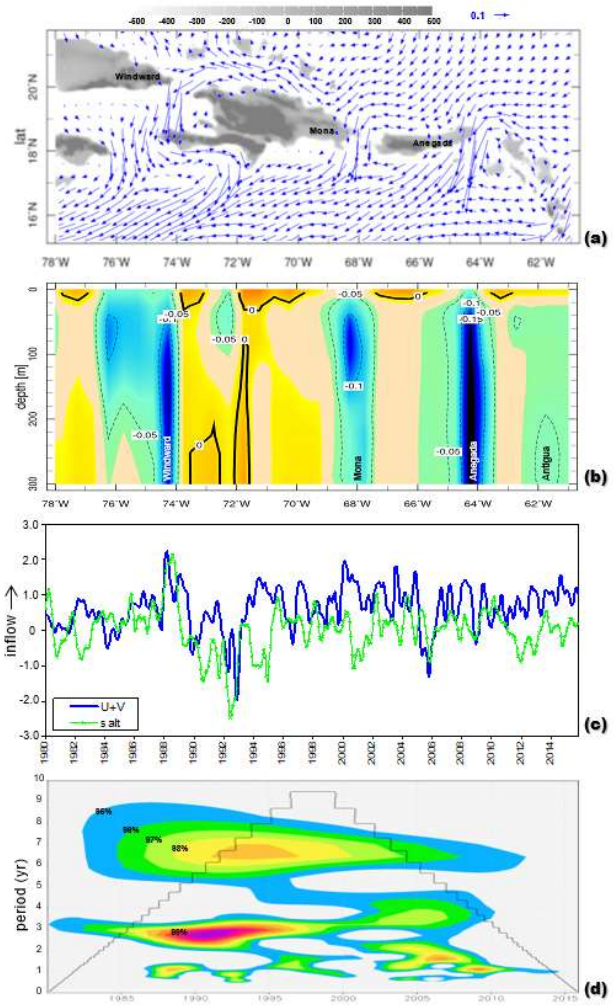


**Figure 2.** (**a**) EOF mode-1 of 5–200 m U and V current vectors with elevation > −500 m grey-shaded, (**b**) depth section of mean minimum V currents over 17.5–19.5° N (blue southward, yellow northward, m/s), (**c**) monthly EOF time-score representing inflow + (blue) and 1–100 m salinity departures, and (**d**) wavelet spectral energy of EOF time-score shaded from 95% (blue) to 99% (red) confidence.

Intra-seasonal fluctuations appeared to be triggered by annual oscillations of currents and winds, estimated from daily HYCOM and EU-marine altimetry. Ocean Rossby waves were detected via daily hovmoller SSHdt analysis in the latitude band 15–17° N in the period 2015–2019. The results proceed from monthly space-time patterns and regional associations to daily modulation of northern Caribbean inflow. Coupled data assimilation and cluster methods reduce uncertainty, despite advances in satellite technology and daily over-sampling. This study was motivated by the realization that marine climate change is sensitive to poleward heat advection in the tropical Atlantic, fed through the Caribbean Sea.

## 3. Results

Context is provided by Appendix A Figure A1 for mean passage currents that identifies place names. Figure A2 compares near-surface meridional currents in the AMW index area for three ocean reanalyses, underpinned by ever-increasing polar-orbiting satellite altimeters <space.oscar.wmo.int/gapanalyses?mission=13>. SODA3 reacts differently in the early 1990s, but all three gradually conform thereafter. Maps of the marine climate are given in Figure 1a–d in the form of SSH, SST, wind, heat flux, and salinity. They illustrate standing anticyclonic eddies southwest of the AMW Passages, which recirculate waters warmed in the Antilles Island wind shadows, with consequences for tropical weather.

### *3.1. EOF Analysis of Currents*

The northern Caribbean inflow variability is characterized by EOF of monthly SODA3 5–200 m U and V currents. Modes 1–5 variance decreases in steps from 29, 11, 7, 6, and 5%. The mode-1 pattern (Figure 2a) reveals sympathetic jets and eddies near each passage. The noisy Atlantic currents contrast with steady westward 'pulling' by the Caribbean Current.

The depth section of V currents (Figure 2b) reveals narrow jets in the AMW Passages, peak southward values of 0.2 m/s from 50–250 m, and wind-driven northward transport above 30 m. The EOF mode-1 time-score (Figure 2c) exhibits pulsing with weak inflow in 1992 and 2005. Its wavelet spectral energy (Figure 2d) has significant periods at 1, 3, and 6.5 years; annual cycling peaks during summer (June). The EOF time-score was found to be uncorrelated with traditional indices that describe Pacific ENSO and North Atlantic climate, e.g., Nino3, SOI, AMO, and NAO. As such, climate teleconnections with Caribbean inflow may be unique and therefore explored by point-to-field regression mapping.

### *3.2. Regression/Composites with AMW Inflow*

The monthly EOF1 time-score regressions onto SLP and netOLR fields reveal a strengthened North Atlantic high and dry climate (as indicated by +netOLR) with respect to (+) high AMW inflow, coupled with a sub-tropical cool/mid-latitude warm SST pattern (Figure 3a,b,c). The trade-winds accelerate over the southern Caribbean during high inflow. The SSHdt and net heat flux regression maps (Figure 3d,e) show high values from Cuba to the Bahamas, as required for geostrophic support to AMW inflow. Compositing the high minus low months (listed in Table 2a) we find strengthened NE trade-winds near South America (Figure 3f) and a SW trough over the Gulf Stream. Salinity increases across the Caribbean (Figure 3g) due to more (less) advection from the AMW (Grenada) Passages (Figure 3h). The AMW inflow is 'pulled' by Caribbean winds in addition to being 'pushed' by the ocean conveyor and its eddies. The composite current anomalies (Figure 3h) suggest the AMW inflow coalesces westward, then splits near Jamaica into a return current off Venezuela and Yucatan outflow.

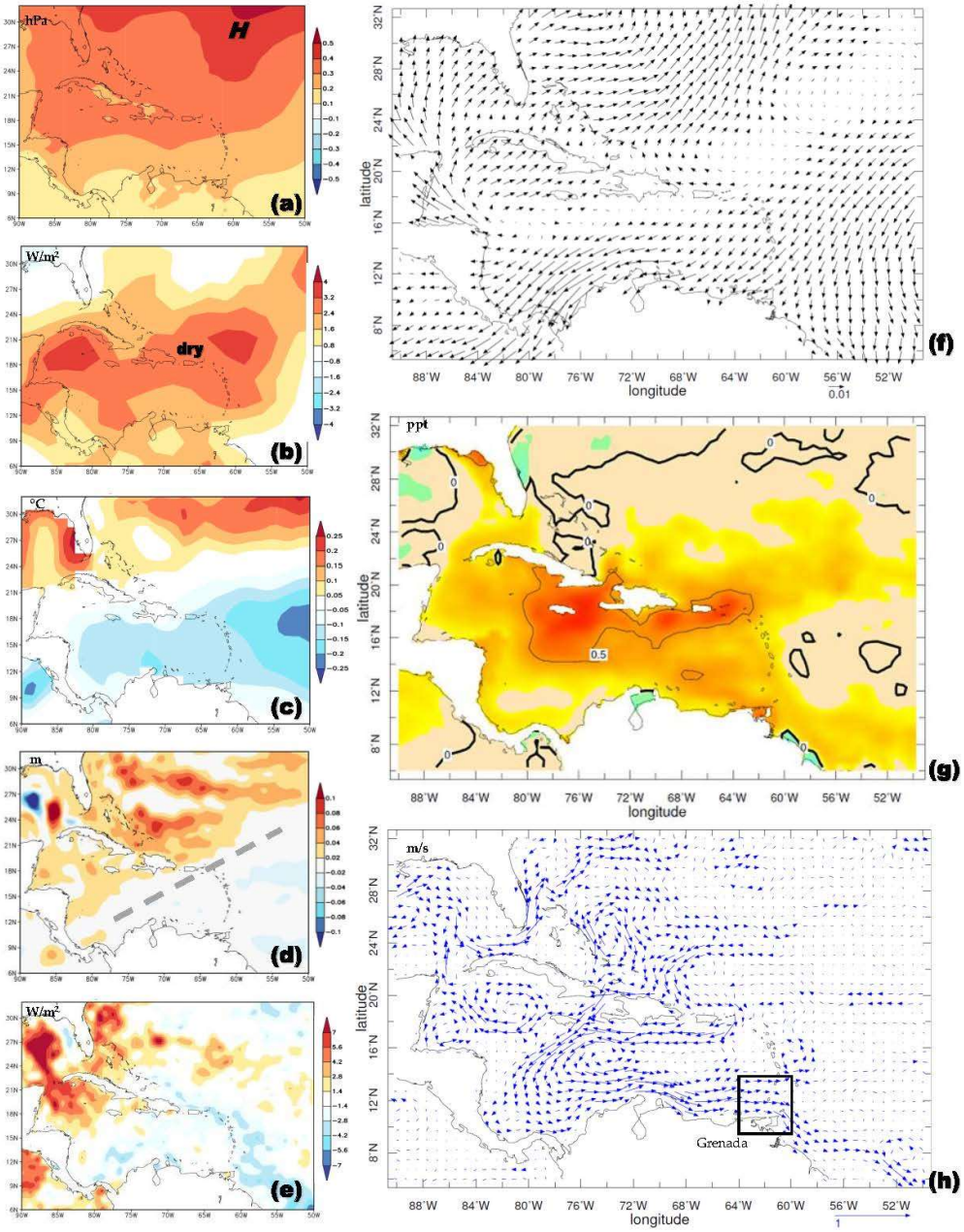


**Figure 3.** Regression of monthly current EOF mode-1 score for the period 1980–2015 onto monthly field anomalies of: (**a**) SLP, (**b**) netOLR, (**c**) SST, (**d**) SSH, (**e**) net heat flux, N = 430. Right column, composite high minus low inflow (based on Table 2a): (**f**) SODA3 wind stress (N/m$^2$), (**g**) 1–100 m salinity, (**h**) 5–200 m currents, with Grenada index box. Label in (**a**) is high pressure; diagonal line in (**d**) denotes the SW-oriented SSH ridge. Insignificant field values are neutral shaded, units are listed in upper left of panels.

The above work using monthly reanalysis has characterized inter-annual features. In the following section, daily upper ocean reanalysis data are employed to describe mesoscale structure and intra-seasonal behavior.

### *3.3. Characteristics of Anegada inflow*

Anegada inflow is deep, narrow, and strong (cf. Figure 2b), and the focus of daily analysis. HYCOM 100 m currents (Figure 4a) show channeling in the passage between Anegada and St Croix with standing eddies on either side. The daily Anegada inflow time series and wavelet spectral energy (Figure 4b,c) reveal transient pulsing in two bands:

40–50 days and 90–120 days, the former likely related to equatorial eastward moving convection (Madden-Julian Oscillation), and the latter to rings in the North Brazil Current. Point-to-field regression maps with respect to the daily Anegada inflow illustrate strengthening of the North Atlantic high (Figure 4d), enhanced trade winds from the Antilles to Panama (Figure 4e), and a drier climate (Figure 4f) indicative of evaporative cooling. Thus, similar processes govern inter-annual and intra-seasonal pulsing of inflow.

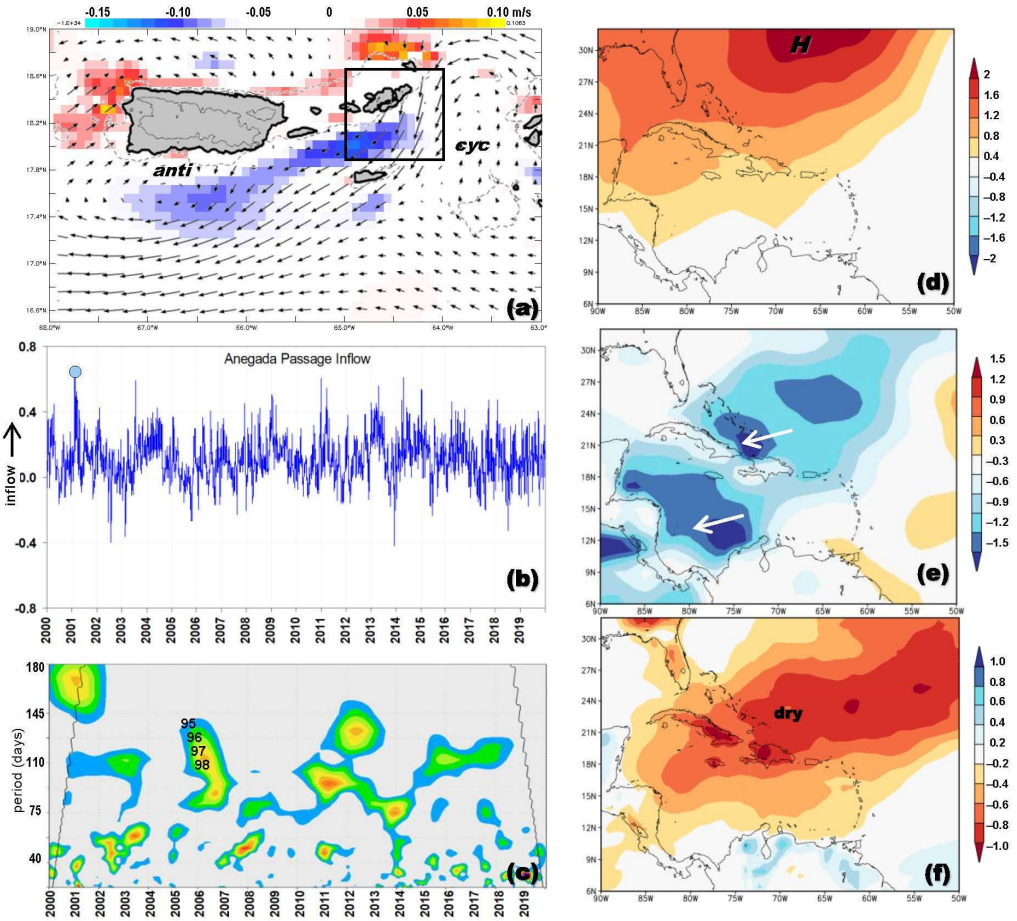


**Figure 4.** (**a**) Mean 100 m current vectors and U component (shaded) around the Anegada Passage with standing eddies labelled. (**b**) Time series of daily Anegada inflow (box in **a**) and its (**c**) wavelet spectral energy shaded from 95% to 99% confidence. Right column: regression of daily Anegada inflow time series onto field anomalies of: (**d**) ERA5 SLP, (**e**) surface zonal wind, (**f**) ERA5 dewpoint Temp, N = 7300. Dot on time series (**b**) is case analyzed in Figure 6. Insignificant field values are neutral shaded.

### 3.4. Ocean Rossby Waves

The regression of AMW inflow onto the large-scale circulation revealed modulation by downstream trade-winds (cf. Figure 4e) which may be coupled with ocean Rossby waves in Caribbean latitudes [46–48]. These are characterized by spectral energy at intra-seasonal to annual periods, characteristic wavelengths from 1000 to 4000 km, and westward phase speeds of ~0.1 m/s. Counter-rotating gyres, associated with annual ocean Rossby waves that emanate from the equatorial Atlantic, alternately enhance and suppress NBC retroflection and the ocean conveyor.

In Figure 5a the mean annual cycle of inflow/outflow currents and trade-winds is analyzed from filtered daily records. The Grenada inflow and Yucatan outflow exhibit annual peaks at the end of May and end of July, a two-month lag over a distance of ~2500 km. The mean annual cycle of surface wind vorticity over the east Atlantic identifies the off-equatorial 'curl' in late summer that initiates annual ocean Rossby waves (Figure 5b).

The line of zero wind vorticity oscillates from 1° N to 9° N from spring to autumn each year, with an alternating pulse in late summer whose amplitude reaches $10^{-4}$ $s^{-1}$. The generation and westward passage of ~4000 km long Rossby waves are evident in the hovmoller analysis (Figure 5c). –SSHdt troughs reach the eastern Caribbean each summer, then crests form in longitudes 60–80° W (+SSHdt) and continue westward at 0.1 m/s with typical wavelengths of ~1000 km. The long-trough/short-crest transformation along the northern flank of the Caribbean Current derives from anticyclonic shear of zonal winds and currents (–dU/dy) which modulates the basin circulation and, together with vertical motions and heat fluxes [49,50], the size of the west Atlantic warm pool.

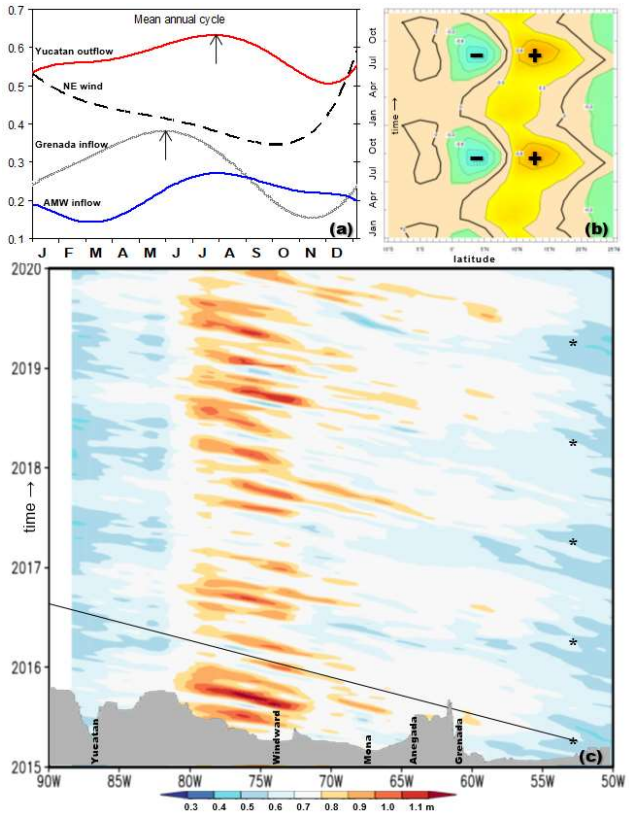


**Figure 5.** (**a**) Mean annual cycle of inflows and outflow (m/s) and NE winds ÷10 (+ westward m/s); arrows highlight two-month lag. (**b**) Hovmoller plot of the mean annual cycle ×2 of surface wind vorticity ($10^{-4}$ $s^{-1}$) averaged over the east Atlantic 15–45°W (+ cyclonic). (**c**) Hovmoller plot of daily SSHdt along 16° N in the period 2015–19, revealing annual troughs (*) and intra-seasonal crests of ocean Rossby waves propagating westward at 0.1 m/s (line) with schematic bathymetry and passages (lower).

### 3.5. Anegada Inflow Case

The peak case of Anegada inflow on 12 February 2001 (cf. Figure 4b, Table 2b) is analyzed in Figure 6a–c. The San Juan radiosonde profile (Figure 6a) during this winter-time surge of trade-winds was capped by a dry layer above 800 hPa (2 km). The shallow airflow was channeled between the mountainous Antilles islands leaving wind shadows downstream. The surface winds had an ENE orientation within an atmospheric boundary layer > 1000 m (Figure 6b). HYCOM 100 m currents on 12 February 2001 illustrate south-westward inflow near St Croix and shear-edge eddies ~100 km west/east of the Anegada Passage (Figure 6c). Four days later (Figure 6d) the inflow had penetrated well into the Caribbean as eddies shifted westward. This event serves to highlight the drivers of inflow: surging trade-winds and favorable counter-rotating current eddies.

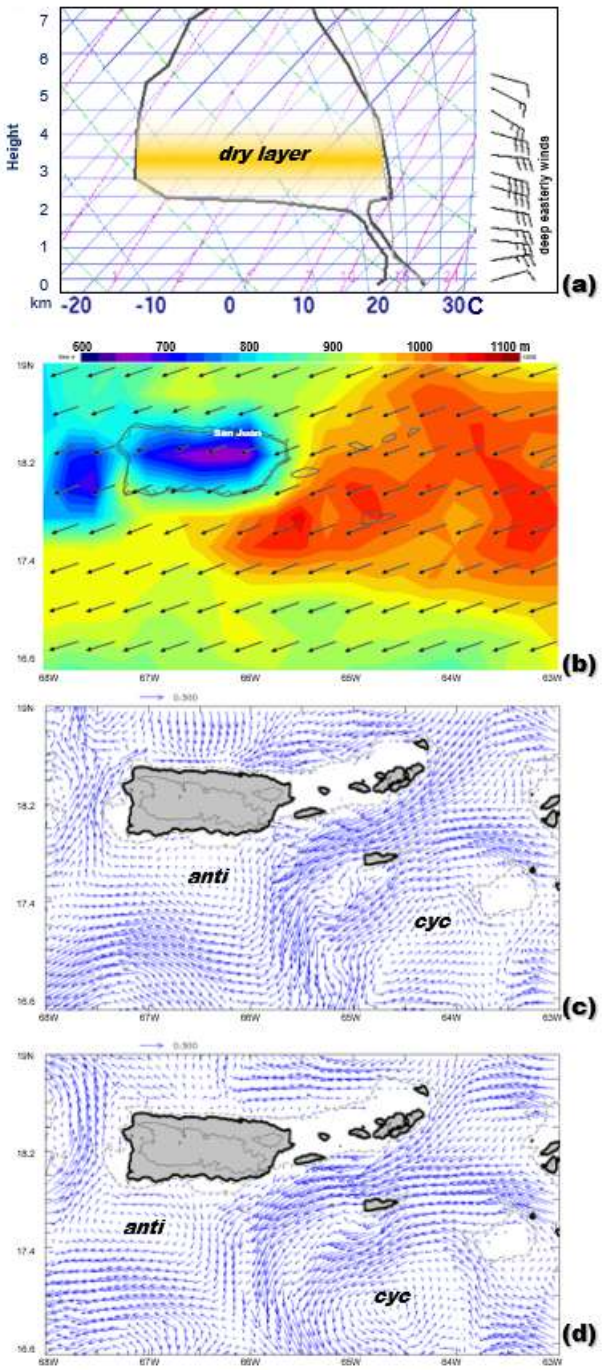


**Figure 6.** Anegada inflow case of 12 February 2001 (cf. Figure 4b): (**a**) San Juan radiosonde skew-Temperature plot and wind profile, (**b**) ERA5 atmospheric boundary layer height and surface wind vectors. (**c**,**d**) HYCOM 100 m currents on 12 February and 16 February, with rotating eddies labelled; contours refer to dashed bathymetry/solid topography.

## 4. Conclusions

Marine climate change involves heat advected poleward by currents along the western edge of the tropical Atlantic, fed through the Caribbean Sea. Consequently, the study of inflows through narrow passages is of great interest. This research has uncovered how ocean–atmosphere coupling affects inflows entering the northern Caribbean in a novel way via reanalysis products underpinned by satellite data assimilation.

Inflow to the Anegada, Mona, Windward (AMW) Passages peaks at ~100 m depth at ~0.2 m/s during summer. Downstream eddies next to Antilles Island wind shadows

deepen the mixed layer (cf. Figure 1c,d) under a surplus heat budget (+30 W/m$^2$) that yields SST > 28°C (Figure 1b) and tropical cyclones [51,52]. Increased AMW inflow was traced to a strengthened high pressure, NE trade-winds, and dry weather resulting in a cooler saltier Caribbean (cf. Figure 3c,g); and a SW-oriented ridge (Figures 3d,f and 4d,e) resembling the atmospheric pattern of north Atlantic Rossby wave-breaking [53]. Annual inflow to the Grenada Passage precedes Yucatan outflow by ~2 months, yet multi-year variability of AMW inflow was uncorrelated with descriptors of Pacific ENSO and North Atlantic forcing: Nino3, SOI, AMO, and NAO.

Composite analysis (Figure 3h) demonstrated that inter-annual surges of inflow to the northern Caribbean tended to oppose Grenada inflow, and thus contribute to a cooler saltier ocean that favors reduced atmospheric convection at ~3 year intervals (Figures 2d and 3b). The AMW inflow spectra (cf. Figure 4c) contained intra-seasonal pulses attributable to tropical convective waves, eddies in the North Brazil Current, and trans-Atlantic ocean Rossby waves (Figure 5c). These features accentuate the multi-year surge and ebb of Atlantic inflow to the northern Caribbean and modulate the downstream warm pool and overlying atmospheric convection. Coupled high-resolution forecasts, underpinned by data assimilation, can handle these complex phenomena to provide guidance on the impacts of high or low inflow to the Caribbean Sea.

**Funding:** This research received no external funding.

**Institutional Review Board Statement:** Not applicable.

**Informed Consent Statement:** Not applicable.

**Data Availability Statement:** A spreadsheet of data analysis is available from the author on request.

**Acknowledgments:** The IRI Climate Library, KNMI Climate Explorer, Univ Hawaii APDRC websites enabled data extraction and analysis.

**Conflicts of Interest:** The author declares no conflict of interest.

## Appendix A

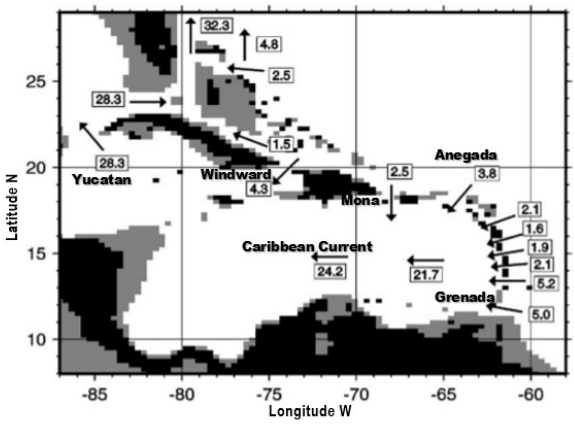


**Figure A1.** Passage flows (Sv) around the Caribbean adapted from [22].

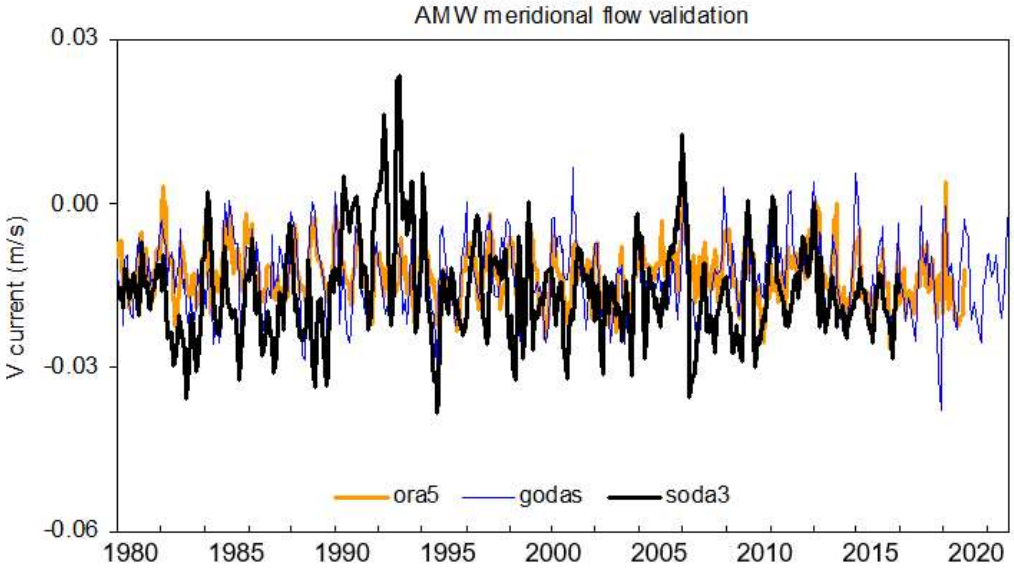


**Figure A2.** Intercomparison of monthly 50–100 m meridional currents averaged over the AMW index area (15–22° N, 78–61° W), a validation that offers context. ORA5 and GODAS are ECMWF and NCEP ocean reanalyses, respectively. Here, Atlantic inflow to the Caribbean is –V.

## References


1. Curry, R.G.; McCartney, M.S. Ocean Gyre Circulation Changes Associated with the North Atlantic Oscillation*. *J. Phys. Oceanogr.* **2001**, *31*, 3374–3400. [CrossRef]
2. Hurrell, J.W.; Visbeck, M.; Busalacchi, A.; Clarke, R.A.; Delworth, T.; Dickson, R.R.; Johns, W.E.; Koltermann, K.P.; Kushnir, Y.; Marshall, D.; et al. Atlantic Climate Variability and Predictability: A CLIVAR Perspective. *J. Clim.* **2006**, *19*, 5100–5121. [CrossRef]
3. Ba, J.S.; Keenlyside, N.S.; Latif, M.; Park, W.; Ding, H.; Lohmann, K.; Mignot, J.; Menary, M.; Otterå, O.H.; Wouters, B.; et al. A multi-model comparison of Atlantic multidecadal variability. *Clim. Dyn.* **2014**, *43*, 2333–2348. [CrossRef]
4. Buckley, M.W.; Marshall, J. Observations, inferences, and mechanisms of the Atlantic Meridional Overturning Circulation: A review. *Rev. Geophys.* **2016**, *54*, 5–63. [CrossRef]
5. Hurrell, J.W.; Van Loon, H. Decadal variations in climate associated with the north atlantic oscillation. *Clim. Chang.* **1997**, *36*, 301–326. [CrossRef]
6. Visbeck, M.; Cullen, H.; Krahmann, G.; Naik, N. An ocean model's response to North Atlantic Oscillation–like wind forcing. *Geophys. Res. Lett.* **1998**, *25*, 4521–4524. [CrossRef]
7. Wang, C. ENSO, Atlantic climate variability, and the Walker and Hadley circulations. In *The Hadley Circulation: Past, Present and Future*; Diaz, H.F., Bradley, R.S., Eds.; Springer: Dordrecht, The Netherlands, 2004; pp. 173–202.
8. Yeshanew, A.; Jury, M.R. North African climate variability. Part 2: Tropical circulation systems. *Theor. Appl. Clim.* **2007**, *89*, 37–49. [CrossRef]
9. Yang, S.; Li, Z.; Yu, J.-Y.; Hu, X.; Dong, W.; He, S. El Niño-Southern Oscillation and its impact in the changing climate. *Natl. Sci. Rev.* **2018**, *5*, 840–857. [CrossRef]
10. Garzoli, S.; Ffield, A.; Yao, Q. NBC retroflection and rings. In *Interhemispheric Water Exchanges in the Atlantic Ocean*; Elsevier Oceanogr Series; Elsevier: Amsterdam, The Netherlands, 2003; Volume 68, pp. 357–374.
11. Garzoli, S.; Ffield, A.E.; Johns, W.; Yao, Q. North Brazil Current retroflection and transports. *J. Geophys. Res.* **2004**, *109*. [CrossRef]
12. Johns, W.E.; Lee, T.N.; Schott, F.A.; Zantopp, R.J.; Evans, R.H. The North Brazil Current retroflection: Seasonal structure and eddy variability. *J. Geophys. Res.* **1990**, *95*, 22103–22120. [CrossRef]
13. Richardson, P.L.; Hufford, G.E.; Limeburner, R.; Brown, W.S. North Brazil Current retroflection eddies. *J. Geophys. Res.* **1994**, *99*, 5081–5093. [CrossRef]
14. Didden, N.; Schott, F. Eddies in the North Brazil Current retroflection region observed by Geosat altimetry. *J. Geophys. Res.* **1993**, *98*, 20121–20131. [CrossRef]
15. Fratantoni, D.M.; Johns, W.E.; Townsend, T.L. Rings of the North Brazil Current: Their structure and behavior inferred from observations and a numerical simulation. *J. Geophys. Res.* **1995**, *100*, 10633–10654. [CrossRef]
16. Goni, G.; Johns, W.E. A census of North Brazil Current rings observed from T/P altimetry: 1992–1998. *Geophys. Res. Lett.* **2001**, *28*, 1–4. [CrossRef]
17. Mertens, C.; Rhein, M.; Walter, M.; Kirchner, K. Modulation of the inflow into the Caribbean Sea by North Brazil Current rings. *Deep. Sea Res. Part I Oceanogr. Res. Pap.* **2009**, *56*, 1057–1076. [CrossRef]
18. Niiler, P.P.; Richardson, W.S. Seasonal variability of the Florida Current. *J. Mar. Res.* **1973**, *31*, 144–167.

19. Schott, F.A.; Lee, T.N.; Zantopp, R. Variability of Structure and Transport of the Florida Current in the Period Range of Days to Seasonal. *J. Phys. Oceanogr.* **1988**, *18*, 1209–1230. [CrossRef]
20. Stalcup, M.C.; Metcalf, W.G. Current measurements in the passages of the Lesser Antilles. *J. Geophys. Res.* **1972**, *77*, 1032–1049. [CrossRef]
21. Wilson, W.D.; Johns, W.E. Velocity structure and transport in the Windward Islands Passages. *Deep. Sea Res. Part I Oceanogr. Res.* **1997**, *44*, 487–520. [CrossRef]
22. Johns, W.E.; Wilson, W.D.; Molinari, R.L. Direct observations of velocity and transport in the passages between the Intra-Americas Sea and the Atlantic Ocean, 1984–1996. *J. Geophys. Res.* **1999**, *104*, 25805–25820. [CrossRef]
23. Leetmaa, A.; Niiler, P.P.; Stommel, H. Does the Sverdrup relation account for the mid-Atlantic circulation? *J. Mar. Res.* **1977**, *35*, 1–10.
24. Schmitz, W.J.; Richardson, P.L. On the sources of the Florida Current. *Deep. Sea Res.* **1991**, *38*, 379–409. [CrossRef]
25. Roemmich, D. The Balance of Geostrophic and Ekman Transports in the Tropical Atlantic Ocean. *J. Phys. Oceanogr.* **1983**, *13*, 1534–1539. [CrossRef]
26. Gordon, A.L. Interocean exchange of thermocline water. *J. Geophys. Res.* **1986**, *91*, 5037–5046. [CrossRef]
27. Rintoul, S. South Atlantic interbasin exchange. *J. Geophys. Res.* **1991**, *96*, 2675–2692. [CrossRef]
28. Gordon, A.L.; Weiss, R.F.; Smethie, W.M.; Warner, M.J. Thermocline and intermediate water communication between the South Atlantic and Indian oceans. *J. Geophys. Res.* **1992**, *97*, 27223–27240. [CrossRef]
29. Schmitz, W.J.; McCartney, M.S. On the North Atlantic Circulation. *Rev. Geophys.* **1993**, *31*, 29–49. [CrossRef]
30. Schott, F.A.; Fischer, J.; Reppin, J.; Send, U. On mean and seasonal currents and transports at the western boundary of the equatorial Atlantic. *J. Geophys. Res.* **1993**, *98*, 14353–14368. [CrossRef]
31. Johns, W.E.; Lee, T.N.; Beardsley, R.; Candela, J.; Castro, B. Annual cycle and variability of the North Brazil Current. *J. Phys. Oceanogr.* **1998**, *28*, 103–128. [CrossRef]
32. Johns, W.E.; Townsend, T.L.; Fratantoni, D.M.; Wilson, W.D. On the Atlantic inflow to the Caribbean Sea. *Deep. Sea Res. Part I Oceanogr. Res. Pap.* **2002**, *49*, 211–243. [CrossRef]
33. Jury, M.R. Slowing of Caribbean through-flow. *Deep. Sea Res. Part II Top. Stud. Oceanogr.* **2020**, *2*, 168. [CrossRef]
34. Stalcup, M.C.; Metcalf, W.G.; Johnson, R.G. Deep Caribbean inflow through the Anegada Passage. *J. Mar. Res.* **1975**, *33*, 15–35.
35. Sturges, W. Mixing of renewal water flowing into the Caribbean Sea. *J. Mar. Res.* **1975**, *33*, 117–130.
36. Fratantoni, D.M.; Zantopp, R.J.; Johns, W.E.; Miller, J.L. Updated bathymetry of the Anegada–Jungfern Passage complex and implications for Atlantic inflow to the abyssal Caribbean Sea. *J. Mar. Res.* **1997**, *55*, 847–860. [CrossRef]
37. Roemmich, D. Circulation of the Caribbean Sea: A well resolved inverse problem. *J. Geophys. Res.* **1981**, *86*, 7993–8005. [CrossRef]
38. Wunsch, C.; Grant, B. Towards the general circulation of the North Atlantic ocean. *Prog. Oceanogr.* **1982**, *11*, 1–59. [CrossRef]
39. Carton, J.A.; Chepurin, G.A.; Chen, L. SODA3: A New Ocean Climate Reanalysis. *J. Clim.* **2018**, *31*, 6967–6983. [CrossRef]
40. Gelaro, R.; McCarty, W.; Suárez, M.J.; Todling, R.; Molod, A.; Takacs, L.; Randles, C.A.; Darmenov, A.; Bosilovich, M.G.; Reichle, R.; et al. The Modern-era retrospective analysis for research and applications, version 2 (MERRA2). *J. Clim.* **2017**, *30*, 5419–5454. [CrossRef]
41. Reynolds, R.W.; Smith, T.M.; Liu, C.; Chelton, D.B.; Casey, K.S.; Schlax, M.G. Daily high-resolution blended analyses for sea surface temperature. *J. Clim.* **2007**, *20*, 5473–5496. [CrossRef]
42. Lee, H.-T. *Climate Algorithm Theoretical Basis Document: Outgoing Longwave Radiation (OLR)*; NOAA CDR Program, CDRP-ATBD-0526; NOAA: Washington, DC, USA, 2014; p. 46.
43. Hersbach, H.; Bell, B.; Berrisford, P.; Hirahara, S.; Horányi, A.; Muñoz-Sabater, J.; Nicolas, J.; Peubey, C.; Radu, R.; Schepers, D.; et al. The ERA5 global reanalysis. *Q. J. R. Meteorol. Soc.* **2020**, *146*, 1999–2049. [CrossRef]
44. Legeais, J.F.; Ablain, M.; Zawadzki, L.; Zuo, H.; Johannessen, J.A.; Scharffenberg, M.G.; Fenoglio-Marc, L.; Fernandes, M.J.; Andersen, O.B.; Rudenko, S.; et al. An improved and homogeneous altimeter sea level record from the ESA climate change initiative. *Earth Syst. Sci. Data* **2018**, *10*, 281–301. [CrossRef]
45. Chassignet, E.P.; Hurlburt, H.E.; Metzger, E.J.; Smedstad, O.M.; Cummings, J.A.; Halliwell, G.R.; Bleck, R.; Baraille, R.; Wallcraft, A.J.; Lozano, C.; et al. US GODAE: Global ocean prediction with the Hybrid coordinate ocean model (HYCOM). *Oceanography* **2009**, *22*, 64–75. [CrossRef]
46. Doos, K. Influence of the Rossby waves on the seasonal cycle in the tropical Atlantic. *J. Geophys. Res.* **1999**, *104*, 29591–29598. [CrossRef]
47. Polito, P.S.; Liu, W.T. Global characterization of Rossby waves at several spectral bands. *J. Geophys. Res.* **2003**, *108*, 3018. [CrossRef]
48. Chu, P.C.; Ivanov, L.M.; Melnichenko, O.V.; Wells, N.C. On long baroclinic Rossby waves in the tropical North Atlantic observed from profiling floats. *J. Geophys. Res.* **2007**, *112*, C05032. [CrossRef]
49. Jouanno, J.; Sheinbaum, J.; Barnier, B.; Molines, J.-M. The mesoscale variability in the Caribbean Sea. Part II: Energy sources. *Ocean Modell.* **2009**, *26*, 226–239.
50. Jury, M.R. Eastern Venezuela coastal upwelling in context of regional weather and climate variability. *Reg. Stud. Mar. Sci.* **2018**, *18*, 219–228. [CrossRef]
51. Lau, K.-M.; Wu, H.-T.; Bony, S. The role of large-scale atmospheric circulation in the relationship between tropical convection and sea surface temperature. *J. Clim.* **1997**, *10*, 381–392. [CrossRef]

52. Jury, M.R. Zonal gradients in the lower atmosphere and upper ocean across Puerto Rico and the windward Antilles in mid-summer 2012. *J. Appl. Meteorol. Climatol.* **2013**, *53*, 731–741. [CrossRef]
53. Zhang, G.; Wang, Z. North Atlantic Rossby wave-breaking during the hurricane season: Association with tropical and extra-tropical variability. *J. Clim.* **2019**, *32*, 3777–3801. [CrossRef]